The 2012 IEEE/ASME International Conference on
Advanced Intelligent Mechatronics
July 11-14, 2012, Kaohsiung, Taiwan

Dynamical Analyses of Humanoid's Walking by Visual Lifting Stabilization Based on Event-driven State Transition

Tomohide Maeba, Mamoru Minami, Akira Yanou, Takayuki Matsuno and Jumpei Nishiguchi

***Abstract*— Biped locomotion created by a controller based on Zero-Moment Point [ZMP] known as reliable control method looks different from human's walking on the view point that ZMP-based walking does not include falling state. However, the walking control that does not depend on ZMP is vulnerable to turnover. Therefore, keeping the event-driven walking of dynamical motion stable is important issue for realization of human-like natural walking. In this paper, walking model of humanoid including slipping, bumping, surface-contacting and point-contacting of foot is discussed, and its dynamical equation is derived by Newton-Euler method. Then, we propose walking stabilizer named "Visual Lifting Stabilization" strategy to enhance standing robustness and prevent the robot from falling down. Simulation results indicate that this strategy helps stabilize pose and bipedal walking even though ZMP is not kept inside convex hull of supporting area.**

I. Introduction

Human beings have acquired an ability of stable bipedal walking in evolving repetitions so far. From a view point of making a stable controller for the bipedal walking based on knowledge of control theory, it looks not easy because of the dynamics with high nonlinearity and coupled interactions between state variables with high dimensions. Therefore how to simplify the complicated walking dynamics to help construct stable walking controller has been studied intensively. Avoiding complications in dealing directly with true dynamics without approximation, inverted pendulum has been used frequently for making a stable controller [1]-[5], simplifying the calculations to determine input torque. Further, linear approximation having the humanoid being represented by simple inverted pendulum enables researchers to realize stable gait through well-known control strategy [6]-[8].

There are two different approaches of humanoid researches such as a real experiment view point and simulation-based one when discussing dynamical walking motion of robot. Using software simulation, it may fall in meaningless discussions unless the dynamical model describes correctly the real physical dynamical behavior. In line with this thinking way, we have discussed a dynamical model of humanoid's walking motion including slipping, bumping and tipping over [9]. Using correct model, simulations enables us to obtain every piece of data without real sensors and can discuss about phenomenon being hard to obtain from real machine, e.g. falling and crashing to floor when walking and jumping. So we think simulation is a convenient tool in discussing complicated walking dynamics before realizing real robot's walking.

As for walking control of the humanoid, ZMP-based walking is known as the most potential approach, which has been proved to be a realistic control strategy to demonstrate stable walking of actual biped robots, since it can guarantee that the robots can keep standing by retaining the zero-moment point within the convex hull of supporting area [10], [11]. Instead of the ZMP, another approaches that put the importance on keeping the robot's walking trajectories inside of a basin of attraction [12]-[14] including a method referring limit cycle to determine input torque [15].

These previous discussions are based on simplified bipedal models, which tend to avoid discussing the effects of feet or slipping existing in real world. Contrarily to the above references, a research [16] has clearly pointed out that the effect of foot bears varieties of the walking gait. [17] has discussed walking gaits in the assumption that walking motion has varieties resulted by its event-driven nature, and the performances have been verified through real-robot-walking experiments. However the humanoid's model in [17] does not have ramification of legs and arms appearing at waist and shoulder, where this presentation is based on a model including the ramifications. Our research has begun from such view point of [16] as aiming at describing gait's dynamics as correctly as possible, including point-contacting state of foot and toe, slipping of the foot and bumping. However, our model differs from [16] and [17] in that it uses leg model without body, on the other hand we discuss the dynamics of whole-body humanoid that contains head, waist and arms. And that what the authors think more important is that the dimension of dynamical equation will change depending on the walking gait's varieties, which has been discussed by [18] concerning one-legged hopping robot. Given as an example that heel be detached from ground while its toe being contacting, a new state variable describing foot's rotation would emerge, resulting in an increase of a number of state variables. In fact, this kind of dynamics with the dimension number of state variables varying by the result of its dynamical time transitions are out of the arena of control theory that discusses how to control a system with fixed states' number. Further the tipping over motion has been called as non-holonomic dynamics that includes a joint without inputting torque, i.e. free joint.

Landing of the heel or the toe of lifting leg in the air to the ground makes a geometrical contact, i.e., algebraic constraint should reduce the dimension of the dynamical

This work was not supported by any organization

The authors are with Graduate School of Natural Science and Technology, Okayama University, 3-1-1 Tsushimanaka, Kita-ku, Okayama, 700-8530, Japan {maeba, minami, yanou, matsuno, nishiguchi}@suri.sys.okayama-u.ac.jp

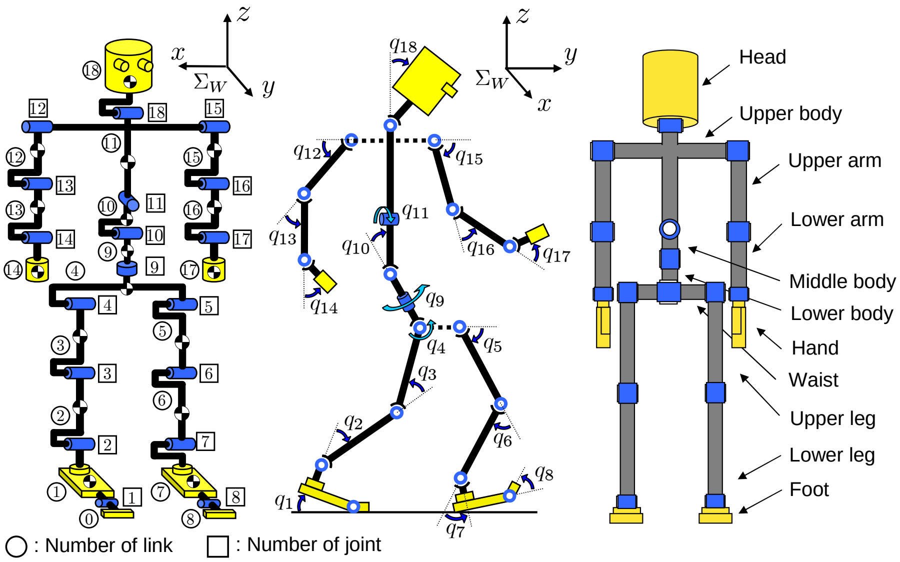

Fig. 1. Definition of humanoid's link, joint and whole body

TABLE I

PHYSICAL PARAMETERS

Link	l_i	m_i	d_i
Head	0.24	4.5	0.5
Upper body	0.41	21.5	10.0
Middle body	0.1	2.0	10.0
Lower body	0.1	2.0	10.0
Upper arm	0.31	2.3	0.03
Lower arm	0.24	1.4	1.0
Hand	0.18	0.4	2.0
Waist	0.27	2.0	10.0
Upper leg	0.38	7.3	10.0
Lower leg	0.40	3.4	10.0
Foot	0.07	1.1	10.0
Total	1.7	63.8	

model [19], [20]. Meanwhile, [21] mentioned how to represent robot's motion contacting with environment that can handle constraint motion with friction by algebraic equation and applied it to human figures. Based on these references, we derive the dynamics of humanoid being simulated as a serial-link manipulator having ramifications by Newton-Euler [NE] method like [22], in which the discussions are leg model and the model has no ramification.

On the other hand, ZMP-independent walking is proposed in this paper to realize human-like natural walking. When ZMP is to be on the edge of convex hull of foot, meaning the humanoid is in a state of tipping over, the gait deems to be unstable, we call this kind of unstable humans' walking as "natural." In line with achieving this natural gaits, we propose a method to enhance standing robustness named "Visual Lifting Stabilization" strategy based on visual servoing concept, referring impedance control method [27]. We utilize real-time pose tracking method to observe an object that is set in front of the robot to measure the robot's head position/orientation based on the object through visual pose estimation [28], [29] during walking. Simulation results show a certain effect that our visual lifting strategy helps realize stabilization of pose and bipedal walking that ZMP is not kept within convex hull of supporting area, which seems to be "natural."

II. DYNAMICAL WALKING MODEL

We discuss a biped robot whose definition is depicted in Fig. 1. Table I indicates length l_i [m], mass m_i [kg] of links and joints' coefficient of viscous friction d_i [N·m·s/rad], which are decided based on [23]. This model is simulated as a serial-link manipulator having ramifications and represents rigid whole body—feet including toe, torso, arms and so on—by 18 degree-of-freedom. Though motion of legs is restricted in sagittal plane, it generates varieties of walking gait sequences since the robot has flat-sole feet and kicking torque. In this paper, one foot including link-0 and link-1 is defined as "supporting-foot" and another foot including link-7 and link-8 is defined as "floating-foot" or "contacting-foot" according to the walking state.

A. Model of Single-foot Standing

Following by NE formulation [24]-[26], we first have to calculate relations of positions, velocities and accelerations between links as forward kinematics procedures from bottom link to top link. Serial link's angular velocity ${}^{i}\boldsymbol{\omega}_i$, angular acceleration ${}^{i}\dot{\boldsymbol{\omega}}_i$, acceleration of the origin ${}^{i}\ddot{\boldsymbol{p}}_i$ and acceleration of the center of mass ${}^{i}\ddot{\boldsymbol{s}}_i$ based on Σ_i fixed at i-th link are obtained as follows.

$$ {}^{i}\boldsymbol{\omega}_i = {}^{i-1}\boldsymbol{R}_i^T\, {}^{i-1}\boldsymbol{\omega}_{i-1} + \boldsymbol{e}_{z_i}\dot{q}_i \quad (1) $$

$$ {}^{i}\dot{\boldsymbol{\omega}}_i = {}^{i-1}\boldsymbol{R}_i^T\, {}^{i-1}\dot{\boldsymbol{\omega}}_{i-1} + \boldsymbol{e}_z\ddot{q}_i + {}^{i}\boldsymbol{\omega}_i \times (\boldsymbol{e}_{z_i}\dot{q}_i) \quad (2) $$

$$ \begin{aligned} {}^{i}\ddot{\boldsymbol{p}}_i = {}^{i-1}\boldsymbol{R}_i^T \Big\{ & {}^{i-1}\ddot{\boldsymbol{p}}_{i-1} + {}^{i-1}\dot{\boldsymbol{\omega}}_{i-1} \times {}^{i-1}\hat{\boldsymbol{p}}_i \\ & + {}^{i-1}\boldsymbol{\omega}_{i-1} \times ({}^{i-1}\boldsymbol{\omega}_{i-1} \times {}^{i-1}\hat{\boldsymbol{p}}_i) \Big\} \end{aligned} \quad (3) $$

$$ {}^{i}\ddot{\boldsymbol{s}}_i = {}^{i}\ddot{\boldsymbol{p}}_i + {}^{i}\dot{\boldsymbol{\omega}}_i \times {}^{i}\hat{\boldsymbol{s}}_i + {}^{i}\boldsymbol{\omega}_i \times ({}^{i}\boldsymbol{\omega}_i \times {}^{i}\hat{\boldsymbol{s}}_i) \quad (4) $$

Here, ${}^{i-1}\boldsymbol{R}_i$ means orientation matrix, ${}^{i-1}\hat{\boldsymbol{p}}_i$ represents position vector from the origin of $(i-1)$-th link to the one of i-th, ${}^{i}\hat{\boldsymbol{s}}_i$ is defined as gravity center position of i-th link and $\boldsymbol{e}_{z_i}$ is unit vector that shows rotational axis of i-th link. However, velocity and acceleration of 4-th link transmit to 9-th link and ones of 11-th link transmit to 12-th, 15-th and 18-th link directly because of ramification mechanisms.

After the above forward kinematic calculation has been done, contrarily inverse dynamical calculation procedures is the next from top to base link. Newton equation and Euler equation of i-th link are represented by Eqs. (5), (6) when ${}^{i}\boldsymbol{I}_i$ is defined as inertia tensor of i-th link.

$$ {}^{i}\boldsymbol{f}_i = {}^{i}\boldsymbol{R}_{i+1}\, {}^{i+1}\boldsymbol{f}_{i+1} + m_i\, {}^{i}\ddot{\boldsymbol{s}}_i \quad (5) $$

$$ \begin{aligned} {}^{i}\boldsymbol{n}_i = & {}^{i}\boldsymbol{R}_{i+1}\, {}^{i+1}\boldsymbol{f}_{i+1} + {}^{i}\boldsymbol{I}_i\, {}^{i}\dot{\boldsymbol{\omega}}_i + {}^{i}\boldsymbol{\omega}_i \times ({}^{i}\boldsymbol{I}_i\, {}^{i}\boldsymbol{\omega}_i) \\ & + {}^{i}\hat{\boldsymbol{s}}_i \times (m_i\, {}^{i}\ddot{\boldsymbol{s}}_i) + {}^{i}\hat{\boldsymbol{p}}_{i+1} \times ({}^{i}\boldsymbol{R}_{i+1}\, {}^{i+1}\boldsymbol{f}_{i+1}) \end{aligned} \quad (6) $$

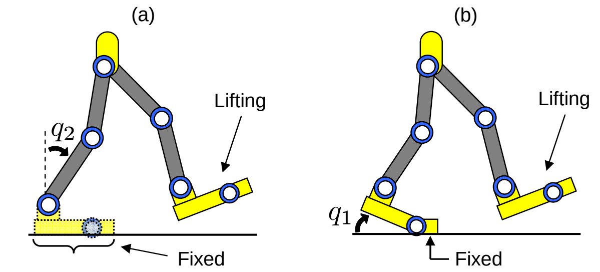

Fig. 2. Gaits including floating-foot

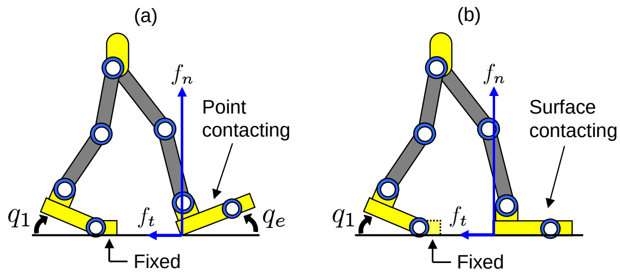

Fig. 3. Gaits including contacting-foot

On the other hand, since force and torque of 5-th and 9-th links are exerted on 4-th link, effects onto 4-th link as:

$$
{}^4\boldsymbol{f}_4 = {}^4\boldsymbol{R}_5{}^5\boldsymbol{f}_5 + {}^4\boldsymbol{R}_9{}^9\boldsymbol{f}_9 + m_4{}^4\ddot{\boldsymbol{s}}_4, \tag{7}
$$

$$
\begin{aligned}
{}^4\boldsymbol{n}_4 = {} & {}^4\boldsymbol{R}_5{}^5\boldsymbol{n}_5 + {}^4\boldsymbol{R}_9{}^9\boldsymbol{n}_9 + {}^4\boldsymbol{I}_4{}^4\dot{\boldsymbol{\omega}}_4 + {}^4\boldsymbol{\omega}_4 \times ({}^4\boldsymbol{I}_4{}^4\boldsymbol{\omega}_4) \\
& + {}^4\hat{\boldsymbol{s}}_4 \times (m_4{}^4\ddot{\boldsymbol{s}}_4) + {}^4\hat{\boldsymbol{p}}_5 \times ({}^4\boldsymbol{R}_5{}^5\boldsymbol{f}_5) \\
& + {}^4\hat{\boldsymbol{p}}_9 \times ({}^4\boldsymbol{R}_9{}^9\boldsymbol{f}_9).
\end{aligned} \tag{8}
$$

Similarly, force and torque of 12-th, 15-th and 18-th links transmit to 11-th link directly. Then, rotational motion equation of i-th link is obtained as Eq. (9) by making inner product of induced torque onto the i-th link's unit vector $\boldsymbol{e}_{z_i}$ around rotational axis:

$$
\tau_i = (\boldsymbol{e}_{z_i})^T\, {}^i\boldsymbol{n}_i + d_i\dot{q}_i. \tag{9}
$$

Finally, we get motion equation with one leg standing as:

$$
\boldsymbol{M}(\boldsymbol{q})\ddot{\boldsymbol{q}} + \boldsymbol{h}(\boldsymbol{q}, \dot{\boldsymbol{q}}) + \boldsymbol{g}(\boldsymbol{q}) + \boldsymbol{D}\dot{\boldsymbol{q}} = \boldsymbol{\tau}, \tag{10}
$$

where, $\boldsymbol{M}(\boldsymbol{q})$ is inertia matrix, $\boldsymbol{h}(\boldsymbol{q}, \dot{\boldsymbol{q}})$ and $\boldsymbol{g}(\boldsymbol{q})$ are vectors which indicate Coriolis force, centrifugal force and gravity, $\boldsymbol{D} = diag[d_1, d_2, \cdots, d_{18}]$ is matrix which means coefficients of joints' viscous friction and $\boldsymbol{\tau}$ is input torque. If supporting-foot is surface-contacting and assumed to be without slipping, joint angle can be thought as $\boldsymbol{q} = [q_2, q_3, \cdots, q_{18}]^T$. This walking pattern is depicted in Fig. 2 (a). When heel of supporting-foot should detach from the ground before floating-foot contacts to the ground as shown in Fig. 2 (b), the state variable for the foot's angle q_1 be added to $\boldsymbol{q}$, thus $\boldsymbol{q} = [q_1, q_2, \cdots, q_{18}]^T$.

B. Model with Contacting Constraints

Giving floating-foot contacts with a ground, contacting-foot like Fig. 3 appears with contacting-foot's position z_h or angle q_e to the ground being constrained. When constraints of foot's position and also foot's rotation are defined as C_1 and C_2 respectively, these constraints are represented by Eq. (11), where $\boldsymbol{r}(\boldsymbol{q})$ means the contacting-foot's heel or toe position in Σ_W.

$$
\boldsymbol{C}(\boldsymbol{r}(\boldsymbol{q})) = \begin{bmatrix} C_1(\boldsymbol{r}(\boldsymbol{q})) \\ C_2(\boldsymbol{r}(\boldsymbol{q})) \end{bmatrix} = \boldsymbol{0} \tag{11}
$$

Then, robot's equation of motion with external force f_n, friction force f_t and external torque τ_n corresponding to C_1 and C_2 can be derived as:

$$
\begin{aligned}
\boldsymbol{M}(\boldsymbol{q})\ddot{\boldsymbol{q}} + \boldsymbol{h}(\boldsymbol{q}, \dot{\boldsymbol{q}}) + \boldsymbol{g}(\boldsymbol{q}) + \boldsymbol{D}\dot{\boldsymbol{q}} & \\
= \boldsymbol{\tau} + \boldsymbol{j}_c^T f_n - \boldsymbol{j}_t^T f_t + \boldsymbol{j}_r^T \tau_n, &
\end{aligned} \tag{12}
$$

where $\boldsymbol{j}_c$, $\boldsymbol{j}_t$ and $\boldsymbol{j}_r$ are defined as:

$$
\boldsymbol{j}_c^T = \left(\frac{\partial C_1}{\partial \boldsymbol{q}^T}\right)^T \left(1 \Big/ \left\| \frac{\partial C_1}{\partial \boldsymbol{r}^T} \right\|\right), \quad \boldsymbol{j}_t^T = \left(\frac{\partial \boldsymbol{r}}{\partial \boldsymbol{q}^T}\right)^T \frac{\dot{\boldsymbol{r}}}{\|\dot{\boldsymbol{r}}\|}, \tag{13}
$$

$$
\boldsymbol{j}_r^T = \left(\frac{\partial C_2}{\partial \boldsymbol{q}^T}\right)^T \left(1 \Big/ \left\| \frac{\partial C_2}{\partial \boldsymbol{q}^T} \right\|\right). \tag{14}
$$

It is common sense that (i) f_n and f_t are orthogonal, and (ii) value of f_t is decided by $f_t = K f_n$ $(0 < K \leq 1)$.

Moreover, differentiating Eq. (11) by time two times, then we can derive the constraint condition of $\ddot{\boldsymbol{q}}$.

$$
\left(\frac{\partial C_i}{\partial \boldsymbol{q}^T}\right)\ddot{\boldsymbol{q}} + \dot{\boldsymbol{q}}^T \left\{ \frac{\partial}{\partial \boldsymbol{q}} \left(\frac{\partial C_i}{\partial \boldsymbol{q}^T}\right) \dot{\boldsymbol{q}} \right\} = 0 \quad (i = 1,\ 2) \tag{15}
$$

Should the $\ddot{\boldsymbol{q}}$ in Eqs. (12), (15) be identical so the time solution of Eq. (15) be under the constraint of Eq. (11), then the following simultaneous equation of $\ddot{\boldsymbol{q}}$, f_n and τ_n have to be maintained during the contacting motion. Here, f_n and τ_n are decided dependently to make the $\ddot{\boldsymbol{q}}$ in Eq. (12) and Eq. (15) be identical.

$$
\begin{bmatrix} \boldsymbol{M}(\boldsymbol{q}) & -(\boldsymbol{j}_c^T - \boldsymbol{j}_t^T K) & -\boldsymbol{j}_r^T \\ \partial C_1/\partial \boldsymbol{q}^T & 0 & 0 \\ \partial C_2/\partial \boldsymbol{q}^T & 0 & 0 \end{bmatrix} \begin{bmatrix} \ddot{\boldsymbol{q}} \\ f_n \\ \tau_n \end{bmatrix}
= \begin{bmatrix} \boldsymbol{\tau} - \boldsymbol{h}(\boldsymbol{q}, \dot{\boldsymbol{q}}) - \boldsymbol{g}(\boldsymbol{q}) - \boldsymbol{D}\dot{\boldsymbol{q}} \\ -\dot{\boldsymbol{q}}^T \left\{ \dfrac{\partial}{\partial \boldsymbol{q}} \left(\dfrac{\partial C_1}{\partial \boldsymbol{q}^T}\right) \right\} \dot{\boldsymbol{q}} \\ -\dot{\boldsymbol{q}}^T \left\{ \dfrac{\partial}{\partial \boldsymbol{q}} \left(\dfrac{\partial C_2}{\partial \boldsymbol{q}^T}\right) \right\} \dot{\boldsymbol{q}} \end{bmatrix} \tag{16}
$$

Here, since motion of the foot is constrained only vertical direction, walking direction has a degree of motion. That is, contacting-foot may slip forward or backward depending on the foot's velocity in traveling direction.

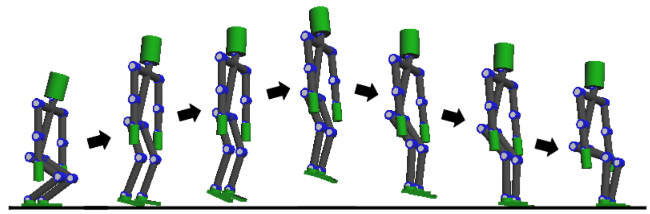

Fig. 4. Example of jumping motion

TABLE II

POSSIBLE STATES OF HUMANOID'S WALKING

S.F.	F.F.	State variables	Constraint
(Stop)			
S	F	$\boldsymbol{q} = [q_2, \cdots, q_n]$	Nothing
S	P	$\boldsymbol{q} = [q_2, \cdots, q_n], f_n$	$C_1 = 0$
S	S	$\boldsymbol{q} = [q_2, \cdots, q_n], f_n, \tau_n$	$C_1, C_2 = 0$
P	F	$\boldsymbol{q} = [q_1, \cdots, q_n]$	Nothing
P	P	$\boldsymbol{q} = [q_1, \cdots, q_n], f_n$	$C_1 = 0$
P	S	$\boldsymbol{q} = [q_1, \cdots, q_n], f_n, \tau_n$	$C_1,\ C_2 = 0$
(Slip)			
S	F	$\boldsymbol{q} = [y_0, q_2, \cdots, q_n]$	Nothing
S	P	$\boldsymbol{q} = [y_0, q_2, \cdots, q_n], f_n$	$C_1 = 0$
S	S	$\boldsymbol{q} = [y_0, q_2, \cdots, q_n], f_n, \tau_n$	$C_1, C_2 = 0$
P	F	$\boldsymbol{q} = [y_0, q_1, \cdots, q_n]$	Nothing
P	P	$\boldsymbol{q} = [y_0, q_1, \cdots, q_n], f_n$	$C_1 = 0$
P	S	$\boldsymbol{q} = [y_0, q_1, \cdots, q_n], f_n, \tau_n$	$C_1, C_2 = 0$
(Air)			
F	F	$\boldsymbol{q} = [y_0, z_0, q_1, \cdots, q_n]$	Nothing
F	P	$\boldsymbol{q} = [y_0, z_0, q_1, \cdots, q_n], f_n$	$C_1 = 0$
F	S	$\boldsymbol{q} = [y_0, z_0, q_1, \cdots, q_n], f_n, \tau_n$	$C_1, C_2 = 0$

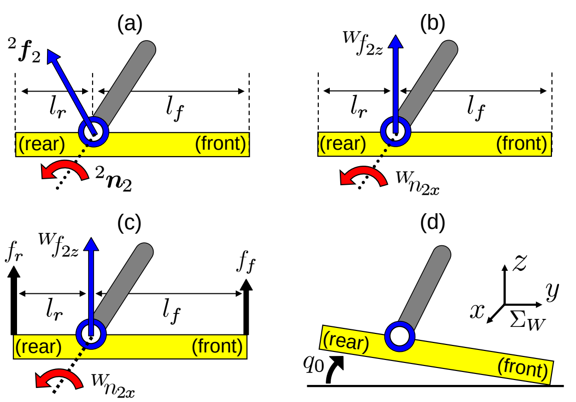

Fig. 6. Force and torque acting on supporting-foot

C. Unified dynamics

As shown in Fig. 2, we distinguish contacting patterns by changing the dimension of state variables. That is, although we do not address the situation that supporting-foot slips or both feet are in the air, Eq. (16) can also represent these dynamics: adding position variable of walking direction y_0 to $\boldsymbol{q}$ in Eq. (16) when supporting-foot begins slipping; and jumping motion by adding further variable of upright direction z_0 to $\boldsymbol{q}$ when jumping represented by Fig. 4.

Table II indicates all possible walking gaits regarding contacting situations—surface-contacting (S), point-contacting (P) and Floating (F)—of supporting-foot (S.F.) and floating-foot or contacting-foot (F.F.). The Table is basically divided into three blocks representing the gait's varieties from a point of states of supporting-foot, such as, "Stop," "Slip" and "Air."

III. WALKING GAIT TRANSITION

Figure 5 depicts all possible gait transition of bipedal walking based on event-driven, which indicate that appropriate dynamics and variables are selected and applied according to the phase or state, which are listed in Table II. In the state that has ramification such as state (II) in Fig. 5 into state (II′) or (III), the gait is switched to next state in case that auxiliary switching condition written above the allow in the figure indicating phase transient is satisfied. In the gait transition from (III) or (III′) to (IV), supporting-foot is switched from one foot to the other foot with renumbering of link, joint and angle's number. What the authors want to emphasize here is that the varieties of this transition completely depend on the solution of dynamics shown as Eq. (10) or Eq. (16).

A. Heel's detaching condition

A condition that heel of supporting-foot detaches from the ground in Fig. 5 (I), (II), (III) to (I′), (II′), (III′) is discussed. For this judging, ${}^2\boldsymbol{f}_2$ and ${}^2\boldsymbol{n}_2$ calculated from Eqs. (5), (6) in case of $i = 2$ are used. Firstly, coordinates of ${}^2\boldsymbol{f}_2$ and ${}^2\boldsymbol{n}_2$ represented by Fig. 6 (a) are converted from Σ_2 to Σ_W. Then, projection to z-axis of the force and projection to x-axis of the torque are derived by using unit vector $\boldsymbol{e}_x = [1, 0, 0]^T$ and $\boldsymbol{e}_z = [0, 0, 1]^T$ as: ${}^W f_{2_z} = \boldsymbol{e}_z^T({}^W\boldsymbol{R}_2{}^2\boldsymbol{f}_2)$, ${}^W n_{2_x} = \boldsymbol{e}_x^T({}^W\boldsymbol{R}_2{}^2\boldsymbol{n}_2)$ like Fig. 6 (b).

Given that supporting-foot's contacting points are to be two of toe and heel as shown Fig. 6 (c), when forces acting on the toe and heel are defined as f_f, f_r, these forces must satisfy the following equations.

$$ {}^W f_{2_z} = f_f + f_r \tag{17} $$

$$ {}^W n_{2_x} = -f_f \cdot l_f + f_r \cdot l_r \tag{18} $$

We can calculate f_f and f_r as Eq. (19) and supporting-foot begins to rotate around the toe like Fig. 6 (d) when value of f_r becomes negative.

$$ f_{f,\ r} = \frac{l_r \cdot {}^W f_{2z}}{l_f + l_r} \pm \frac{{}^W n_{2x}}{l_f + l_r} \tag{19} $$

B. Bumping

When floating-foot attaches to ground, we need to consider bumping motion [16]. Figure 5 has two kinds of bumping concerning heel and toe. We denote dynamics of bumping between the heel and the ground below. By integrating Eq. (12) under $\tau_n = 0$ in time, equation of striking moment can be obtained as follows.

$$ \boldsymbol{M}(\boldsymbol{q})\dot{\boldsymbol{q}}(t_1^+) = \boldsymbol{M}(\boldsymbol{q})\dot{\boldsymbol{q}}(t_1^-) + (\boldsymbol{j}_c^T - \boldsymbol{j}_t^T K)F_{im} \tag{20} $$

Eq. (20) describes the bumping in z-axis of Σ_W between the heel and the ground. $\dot{\boldsymbol{q}}(t_1^+)$ and $\dot{\boldsymbol{q}}(t_1^-)$ are angular velocity after and before the strike respectively. $F_{im} = \lim_{t_1^- \to t_1^+} \int_{t_1^-}^{t_1^+} f_n dt$ means impulse of bumping. Motion of the robot is constrained by the followed equation that is given by differentiating C_1 by time after the strike.

$$ \frac{\partial C_1}{\partial \boldsymbol{q}} \dot{\boldsymbol{q}}(t_1^+) = 0 \tag{21} $$

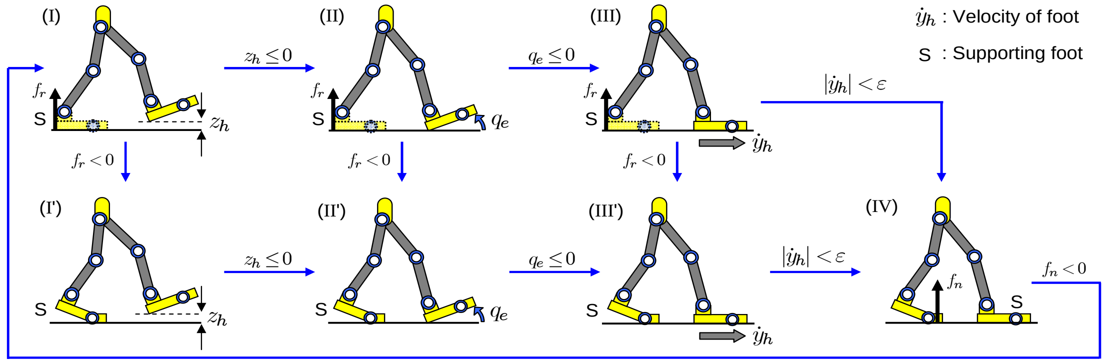

Fig. 5. State and gait's transition

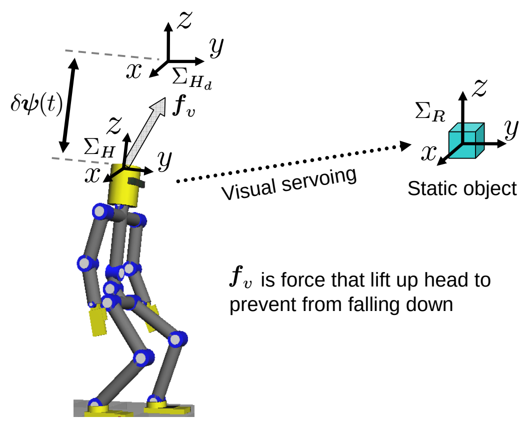

Fig. 7. Concept of Visual Lifting Stabilization

Then, the equation of matrix formation in the case of heel's bumping can be obtained as follows.

$$\begin{bmatrix} \boldsymbol{M}(\boldsymbol{q}) & -(\boldsymbol{j}_c^T - \boldsymbol{j}_t^T K) \\ \frac{\partial C_1}{\partial \boldsymbol{q}^T} & 0 \end{bmatrix} \begin{bmatrix} \dot{\boldsymbol{q}}(t_1^+) \\ F_{im} \end{bmatrix} = \begin{bmatrix} \boldsymbol{M}(\boldsymbol{q})\dot{\boldsymbol{q}}(t_1^-) \\ 0 \end{bmatrix} \tag{22}$$

We can derive the dynamics regarding the toe's bumping based on the similar above process.

IV. Visual Lifting Stabilization

This section propose a vision-feedback control for improving humanoid's standing/walking stability as shown in Fig. 7. We use a model-based matching method to measure pose of a static target object denoted by $\boldsymbol{\psi}(t)$ based on Σ_H, which represents the robot's head. The desired relative pose of Σ_R (reference target object's coordinate) and Σ_H is predefined by Homogeneous Transformation as ${}^{H_d}\boldsymbol{T}_R$. The difference of the desired head pose Σ_{H_d} and the current pose Σ_H is denoted as ${}^{H}\boldsymbol{T}_{H_d}$, it can be described by:

$${}^{H}\boldsymbol{T}_{H_d}(\boldsymbol{\psi}_d(t), \boldsymbol{\psi}(t)) = {}^{H}\boldsymbol{T}_R(\boldsymbol{\psi}(t)) \cdot {}^{H_d}\boldsymbol{T}_R{}^{-1}(\boldsymbol{\psi}_d(t)), \tag{23}$$

where, although ${}^{H}\boldsymbol{T}_R$ is calculated by $\boldsymbol{\psi}(t)$ that can measured by on-line visual pose estimation method [28], [29], we assume this parameter as being detected correctly in this paper. Here, the force exerted on the head to minimize $\delta\boldsymbol{\psi}(t) = \boldsymbol{\psi}_d(t) - \boldsymbol{\psi}(t)$ calculated from ${}^{H}\boldsymbol{T}_{H_d}$—the pose deviation of the robot's head caused by gravity force and walking dynamical influences—is considered to be directly proportional to $\delta\boldsymbol{\psi}(t)$. The joint torque $\boldsymbol{\tau}_h(t)$ that pulls the robot's head up is given the following equation:

$$\boldsymbol{\tau}_h(t) = \boldsymbol{J}_h(\boldsymbol{q})^T \boldsymbol{K}_p \delta\boldsymbol{\psi}(t), \tag{24}$$

where $\boldsymbol{J}_h$ is Jacobian matrix of the head pose against joint angles and $\boldsymbol{K}_p$ means proportional gain similar to impedance control. We use this input to compensate the falling motions caused by gravity or dangerous slipping motion happened unpredictably during all walking states in Fig. 5. Notice that the input torque for non-holonomic joint like q_1 (foot tip joint), τ_{h_1} in $\boldsymbol{\tau}_h(t)$ in Eq. (24) is to be set as zero since it is free joint.

V. Example of Bipedal Walking

Under the environment that sampling time was set as 3.0×10^{-3} [sec] and friction force between foot and the ground as $f_t = 0.7 f_n$, the following simulations were conducted. In regard to simulation environment, we used "Borland C++ Builder Professional Ver. 5.0" to make simulation program and "OpenGL Ver. 1.5.0" to display humanoid's time-transient configurations.

A. Analyses of walking motion

To realize bipedal walking, three kinds of input torques were used. One is Eq. (24) for stabilization of pose. Although $\delta\boldsymbol{\psi}(t)$ can represent error concerning the humanoid's both position and orientation, only position was utilized in this case, so $\boldsymbol{K}_p$ was set as $\boldsymbol{K}_p = diag[20, 290, 1100]^T$. Second is periodical input to thigh of floating-leg (joint-5) to make the leg step forward, which represented as $\tau_5 = 20\cos\{2\pi(t - t_2)/1.85\}$. The other is periodical input to roll angle of body (joint-11) to generate motion of arms, which represented as $\tau_{11} = 50\sin\{2\pi(t - t_2)/1.85\}$. Here, t_2 means the time that supporting-foot and contacting-foot are switched described in section III. However, input for joint-1 was always set are zero like Fig. 12.

By the above inputs, the humanoid could walk as shown in Fig. 8 and we got the following results: average length of stride is 0.45 [m] and walking speed is 2.34 [km/h]. Also upper body is inclined forward during walking because head is pulled obliquely upward by Eq. (24). Figure 9 is the relation between angle q_{10} and angular velocity $\dot{q}_{10}$ of waist. Although both trajectories being close the same constant cycle along with time passage, these trajectories in Fig. 9 are not limit cycle since trajectories have a certain width after 1000 walking steps, meaning these oscillations are strange attractors. We have not known whether these trajectories are chaos or not. Further, Fig. 10 shows the relation between angles $q_{12},\ q_{15}$ and angular velocities $\dot{q}_{12},\ \dot{q}_{15}$ of arms. Here, $q_{12} = q_{15} = 0.2$ [rad] and $\dot{q}_{12} = \dot{q}_{15} = 0.0$ [rad/s] as initial condition, then there was no input torque to arms and hands while walking. However, amplitude of arms's swing became large spontaneously and converged to a certain amplitude and period. Therefore, we can say that both arms' swing were caused by interactions of walking dynamics.

B. Event-driven walking pattern

Figure 11 shows state transition generated by the humanoid's dynamics, both feet's position in y-z plain and displacement of ZMP during one walking step. In this simulation, the humanoid walked in accordance with the following path: (I) $\rightarrow$ (I$'$) $\rightarrow$ (II$'$) $\rightarrow$ (III$'$) $\rightarrow$ (IV) $\rightarrow$ (I) $\rightarrow \cdots$. This transition was selected among all possible transient in Fig. 5 by the solution of dynamics represented by Eqs. (10), (16), initial condition and input torque. That is, the path of transition will be changed easily by these factors.

Moreover, Fig. 11 denotes that ZMP moves forward and reaches the edge of supporting-foot while the other foot in the air, meaning that the robot is tipping over, which does not appear in ZMP-based walking. We think that this kind of natural walking is caused by the effect of visual feedback as shown in the following subsection.

C. Effects of visual feedback

We assume that two patterns of supporting-foot's contacting and input torques based on Eq. (24). Since state of Fig. 12 (a) meaning surface-contacting is thought to be a manipulator fixed at the ground as shown in Fig. 13 (a), it is clear that Eq. (24) can lift the robot's head up toward desired position. On the other hand, effectiveness of visual feedback is unclear in toe-contacting phase because there is no input to toe's joint that means the robot's non-holonomic dynamics include constraint condition of toe's joint. However, Fig. 13 (b) simulating the state of Fig. 12 (b) indicates that although one link corresponding to the foot falls by gravity, the others are pulled toward the desired position. Therefore, we can say that visual feedback may make the whole dynamics stable partially even though non-holonomic constraint be added to.

Here, we discuss whether Eq. (24) makes the humanoid's pose stable. By changing the value of feedback gain $\boldsymbol{K}_p$, the strength of force lifting the robot's head is adjustable. Here, to verify some effects that the strength of visual feedback gives to the humanoid's walking, we confirmed walkings by using some kinds of $\alpha\boldsymbol{K}_p$ (α is weight coefficient). Figure 14 shows vertical position of center of foot's bottom face from 10 to 20 [sec] and Table III means maximum average of the position and period of walking according to the value of α. When α is larger, walking period becomes longer and vertical position of the foot becomes higher, with the robot's head pulled strongly. Moreover, if $0.82 \leq \alpha \leq 1.06$, the humanoid could walk in our simulation conditions.

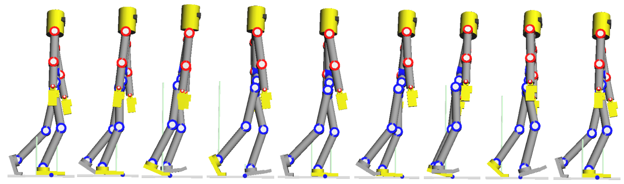

Fig. 8. Screen-shot of bipedal walking

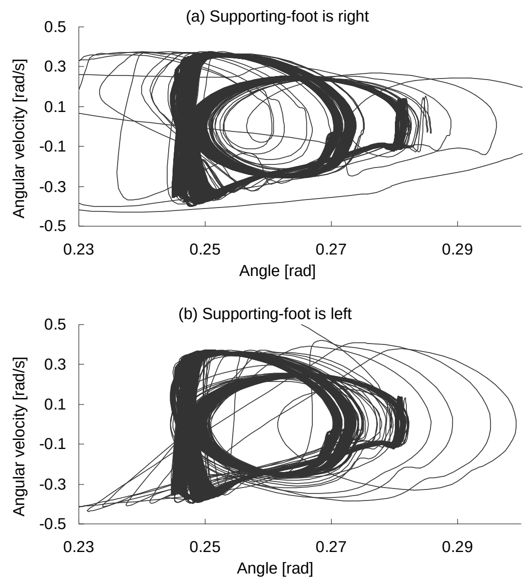

Fig. 9. Relation of q_{10} and $\dot{q}_{10}$

VI. Conclusion

As a first step to realize human-like walking for complicated humanoid's dynamics, strict dynamical model that contains flat feet including toe, slipping and bumping was created in this paper. Then, we proposed Visual Lifting Stabilization based on visual feedback as a strategy that prevents turnover generated by unpredictable slipping or unstable gaits. From simulation results, we confirmed that the proposed strategy can help realize a ZMP-independent walking and verified that walking period and feet's motion of the humanoid change by adjusting the strength of visual feedback. Moreover, through the motion of arms and legs from transient state to steady state, we also verified that left and right arms' swinging motion began spontaneously by the internal dynamical interactions even though their input torques of both arms are set to be always zero, converging to the same symmetric phase diagrams.

For this reason, we believe that this strategy will additionally contribute to analyze humanoid's motion for human-like bipedal walking.

References

[1] S. Kajita, M. Morisawa, K, Miura, S. Nakaoka, K. Harada, K. Kaneko, F. Kanehiro and K. Yokoi, "Biped Walking Stabilization Based on Linear Inverted Pendulum Tracking," *Proc. IEEE/RSJ International Conference on Intelligent Robots and Systems*, pp.4489–4496, 2010.

[2] H. Dau, C. Chew and A. Poo, "Proposal of Augmented Linear Inverted Pendulum Model for Bipedal Gait Planning," *Proc. IEEE/RSJ International Conference on Intelligent Robots and Systems*, pp.172–177, 2010.

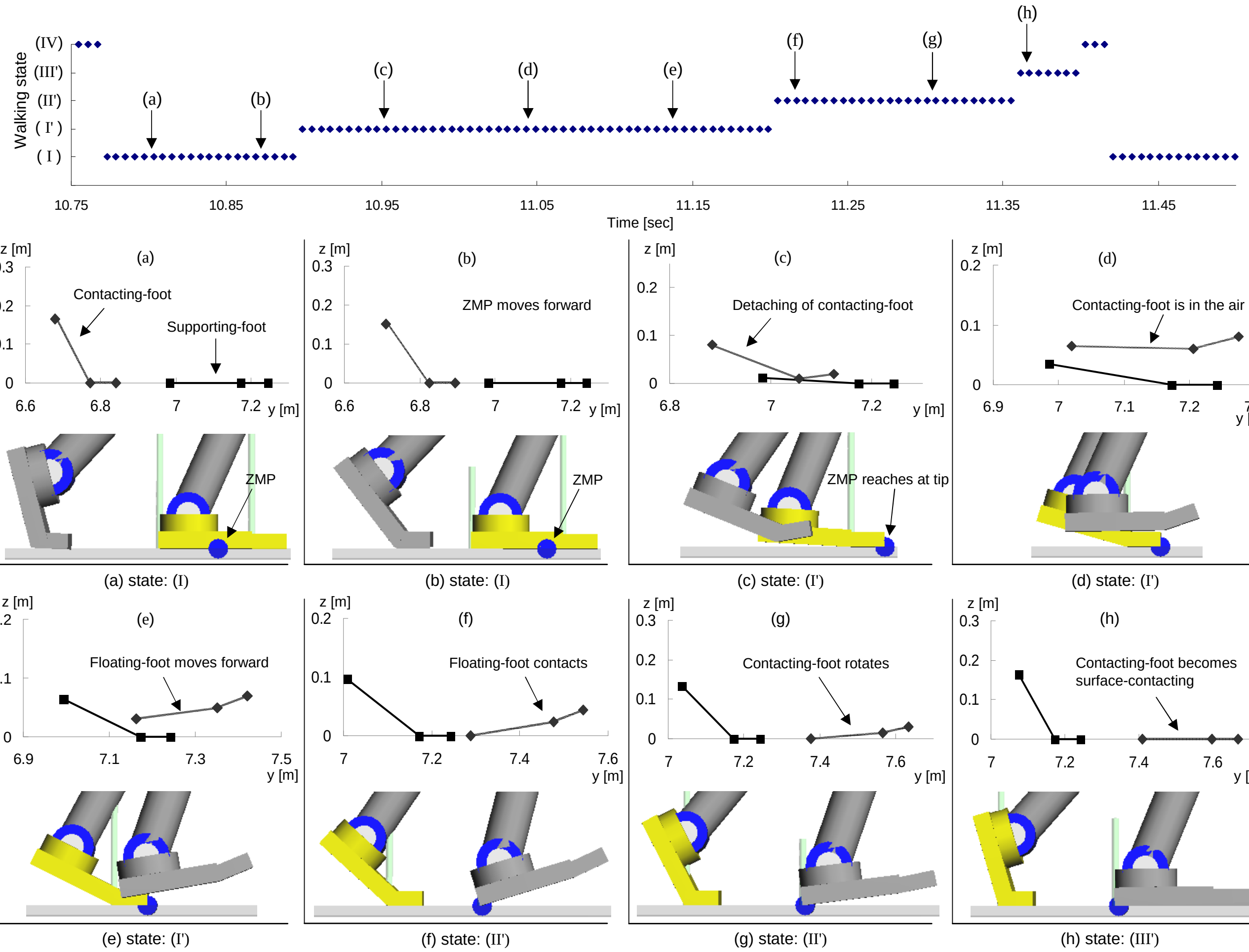

Fig. 11. Feet's position in y-z plain (Σ_W) and displacement of ZMP during one walking step

TABLE III

INFLUENCE BY WEIGHT COEFFICIENT α

The value of α	Period of walking	Maximum vertical position
0.9	1.26 [sec]	0.0533 [m]
1.0	1.38 [sec]	0.0549 [m]
1.5	1.50 [sec]	0.0572 [m]

[3] S. Kajita and K. Tani, "Study of Dynamic Locomotion on Rigged Terrain-Derivation and Application of the Linear Inverted Pendulum Mode," *Proc. IEEE International Conference on Robotics and Automation*, pp.1405–1411, 1991.

[4] S. Kajita, F. Kanehiro, K. Kaneko, K. Yokoi and H. Hirukawa, "The 3D Linear Inverted Pendulum Mode: A simple modeling for a biped walking pattern generation," *Proc. IEEE/RSJ International Conference on Intelligent Robots and Systems*, 2001.

[5] J.H. Park and K.D. Kim, "Biped walking robot using gravity-compensated inverted pendulum mode and computed torque control," *Proc. IEEE International Conference on Robotics and Automation*, Vol.4, pp.3528–3593, 1998.

[6] P.B. Wieber, "Trajectory free linear model predictive control for stable walking in the presence of strong perturbations," *Proc. International Conference on Humanoid Robotics*, 2006.

[7] P.B. Wieber, "Viability and predictive control for safe locomotion," *Proc. IEEE/RSJ International Conference on Intelligent Robots and Systems*, 2008.

[8] A. Herdt, N. Perrin and P.B. Wieber, "Walking without thinking about it," *Proc. IEEE/RSJ International Conference on Intelligent Robots and Systems*, pp.190–195, 2010.

[9] W. Song, M. Minami, T. Maeba. Y Zhang and A. Yanou, "Visual Lifting Stabilization of Dynamic Bipedal Walking," *Proceedings of 2011 IEEE-RAS International Conference on Humanoid Robots*, pp.345-351, 2011.

[10] M. Vukobratovic, A. Frank and D. Juricic, "On the Stability of Biped Locomotion," *IEEE Transactions on Biomedical Engineering*, Vol.17, No.1, 1970.

[11] M. Vukobratovic and J. Stepanenko, "On the Stability of Anthropomorphic Systems," *Mathematical Biosciences*, Vol.15, pp.1–37, 1972.

[12] S. Colins, A. Ruina, R. Tedrake and M. Wisse, "Efficient Bipedal Robots Based on Passive-Dynamic Walkers," *Science*, Vol.307, pp.1082–1085, 2005.

[13] J. Pratt, P. Dilworth and G. Pratt, "Virtual Model Control of a Bipedal Walking Robot," *Proc. IEEE International Conference on Robotics and Automation*", pp.193–198, 1997.

[14] R.E. Westervelt, W.J. Grizzle and E.D. Koditschek, "Hybrid Zero Dynamics of Planar Biped Walkers," *IEEE Transactions on Automatic Control*, Vol.48, No.1, pp.42–56, 2003.

[15] Y. Harada, J. Takahashi, D. Nenchev and D. Sato, "Limit Cycle Based Walk of a Powered 7DOF 3D Biped with Flat Feet," *Proc. of International Conference on IROS*, pp.3623–3628, 2010.

[16] Y. Huang, B. Chen, Q. Wang, K. Wei and L. Wang, "Energetic efficiency and stability of dynamic bipedal walking gaits with different step lengths," *Proc. IEEE/RSJ International Conference on Intelligent Robots and Systems*, pp.4077–4082, 2010.

[17] M. Sobotka and M. Buss, "A Hybrid Mechatronic Tiliting Robot: Modeling, Trajectories, and Control," *Proceedings of the 16th IFAC World Congress*, 2005.

[18] T. Wu, T. Yeh and B. Hsu, "Trajectory Planning of a One-Legged

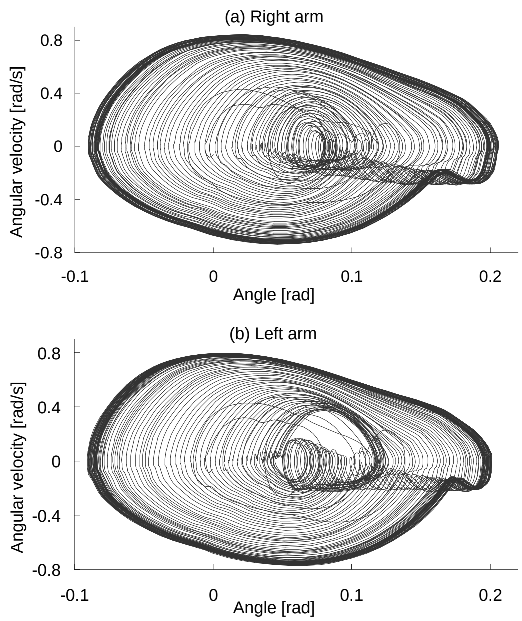

Fig. 10. Motion trajectories of upper arms

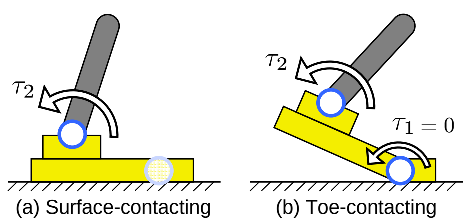

Fig. 12. Input torque for supporting-foot

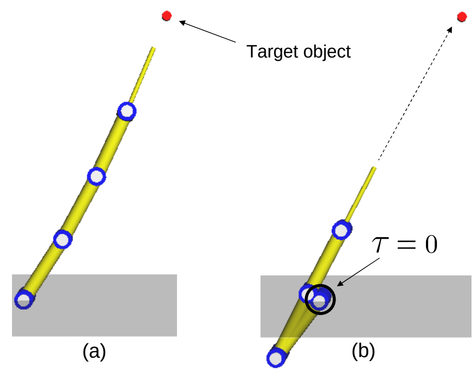

Fig. 13. Verification of visual feedback

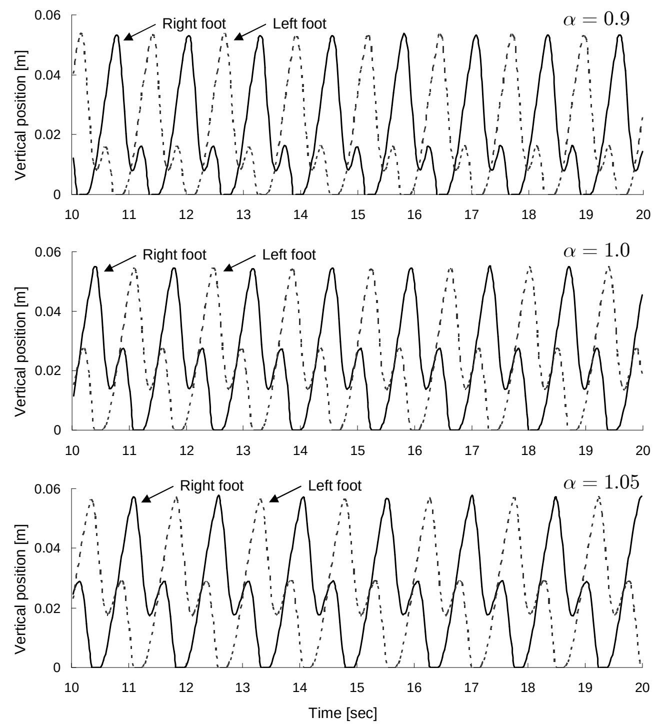

Fig. 14. Feet's vertical position in case of $\alpha = 0.9,\ 1.0,\ 1.05$

Robot Performing Stable Hop," *Proc. IEEE/RSJ International Conference on Intelligent Robots and Systems*, pp.4922–4927, 2010.

[19] H. Hemami and B.F. Wyman, "Modeling and Control of Constrained Dynamic Systems with Application to Biped Locomotion in the Frontal Plane," *IEEE Trans. on Automatic Control*, AC-24-4, pp.526–535, 1979.

[20] C.L. Golliday and H. Hemami, "An Approach to Analyzing Biped Locomotion Dynamics and Designing Robot Locomotion Controls," *IEEE Trans. on Automatic Control*, AC-22-6, pp.963–972, 1997.

[21] Y. Nakamura and K. Yamane, "Dynamics of Kinematic Chains with Discontinuous Changes of Constraints—Application to Human Figures that Move in Contact with the Environments—," *Journal of RSJ*, Vol.18, No.3, pp.435–443, 2000 (in Japanese).

[22] Y. Fujimoto and A. Kawamura, "Three Dimensional Digital Simulation and Autonomous Walking Control for Eight-Axis Biped Robot," *Proc. IEEE International Conference on Robotics and Automation*, pp.2877–2884, 1995.

[23] M. Kouchi, M. Mochimaru, H. Iwasawa and S. Mitani, "Anthropometric database for Japanese Population 1997-98," Japanese Industrial Standards Center (AIST, MITI), 2000.

[24] J.Y.S. Luh, M.W. Walker and R.P.C. Paul, "On-Line Computational Scheme for Mechanical Manipulators," *ASME J. of DSME*, Vol.102, No.2, pp.69–76, 1980.

[25] M.W. Walker and D.E. Orin, "Efficient Dynamic Computer Simulation of Robotic Mechanisms," *ASME J. of DSME*, Vol.104, pp.205–211, 1982.

[26] T. Mita and K. Osuka, "Introduction to Robot Control," CORONA PUBLISHING CO., LTD., 1989 (in Japanese).

[27] N. Hogan, "Impedance Control; An Approach to Manipulation, Parts I–III, *ASME Journal of Dynamics Systems, Measurement, and Control* Vol.107, No.1, pp.1–24, 1985.

[28] W. Song, M. Minami, F. Yu, Y. Zhang and A. Yanou, "3-D Hand & Eye-Vergence Approaching Visual Servoing with Lyapunov-Stable Pose Tracking," *Proceedings of IEEE International Conference on Robotics and Automation*, pp.5210–5217, 2011.

[29] F. Yu, W. Song and M. Minami, "Visual Servoing with Quick Eye-Vergence to Enhance Trackability and Stability," *Proceedings of IEEE/RSJ International Conference on Intelligent Robots and Systems*, pp.6228–6233, 2010.